

## AUTOMATED AERODYNAMIC OPTIMIZATION SYSTEM FOR SST WING-BODY CONFIGURATION

Daisuke SASAKI\*, Guowei YANG† and Shigeru OBAYASHI‡

Tohoku University, Sendai 980-8577, JAPAN

### Abstract

In this paper, wing-body configurations for a next generation Supersonic Transport are designed by means of Multiobjective Evolutionary Algorithms. SST wing-body configurations are designed to reduce the aerodynamic drag and the sonic boom for supersonic flight. To lower the sonic boom strength, the present objective function is to satisfy the equivalent area distribution for low sonic boom proposed by Darden. Wing and fuselage is defined by 131 design variables and optimized at the same time. Structured multiblock grids around SST wing-body configuration are generated automatically and an Euler solver is used to evaluate the aerodynamic performance of SST wing-body configuration. Compromised solutions are found as Pareto solutions. Although they have a variety of fuselage configurations, all of them have a similar wing planform due to the imposed constraints. The present results imply that a lifting surface should be distributed innovatively to match Darden's distribution for low boom.

### 1. Introduction

To develop a next generation Supersonic Transport (SST), many researches have been performed.<sup>1-10</sup> However, the next generation SST still has many technical requirements to be achieved. One of them is high aerodynamic efficiency for an economic flight, and another is low sonic boom for an environmental issue. These demands have tradeoff, because the reduction of sonic boom often leads to the increase of drag. To satisfy these demands, multiobjective (MO) optimization has been performed in the present optimization by using Multiobjective Genetic Algorithms (MOGAs).

To identify such tradeoffs in detail, MO optimization must be performed. MO optimization seeks to optimize the components of a vector-valued objective function unlike the single objective

optimization. Pareto solutions, which are members of the Pareto-optimal set obtained by solving MO problems, represent tradeoffs among multiple objectives. Since an application of Evolutionary Algorithms (EAs) to MO problem has many advantages, such methods have been increasingly used in aerodynamic optimization problems.<sup>9-12</sup> MOGAs can sample multiple Pareto solutions efficiently and effectively. Since GAs seek optimal solutions in parallel using a population of design candidates, MOGAs can identify multiple Pareto solutions at the same time without specifying weights between objectives. Objective functions can be evaluated by the existing CFD solver without any modification.

National Aerospace Laboratory of Japan (NAL) designed a scaled supersonic experimental airplane for NEXST-I project.<sup>3</sup> The plane is composed of fuselage, wing and tail. The wing is designed to achieve Natural Laminar Flow over the wing and the fuselage is designed based on the area rule. The resulting wing-body configuration has good aerodynamic performance. To account for the low boom, the fuselage is then modified to have the nonsymmetric cross section for NEXST-II.<sup>6</sup> NAL also have a SST-CFD Workshop every two years. At 3rd SST-CFD-Workshop in 2001, a design competition of SST was held. The present optimization is based on the assignments used there. The objective is to improve L/D, and an optional objective is to reduce sonic boom under given constraints.

In our previous research, the isolated wing shape was designed.<sup>10</sup> The aircraft was assumed to cruise at a supersonic speed only over the sea and to cruise at a transonic speed over the land to avoid sonic boom generation over the population area. This means the important design objectives are not only to improve a supersonic cruise performance but also to improve a transonic one. Then both aerodynamic drags were minimized under lift constraints, and the bending moment at the wing root was also minimized to prevent all the Pareto solutions having impractically large aspect ratios. In addition, the minimization of a pitching moment was introduced as the fourth objective function to reduce the pitching moment associated with a highly swept wing. A Navier-Stokes solver was used to evaluate the wing performance at both supersonic and transonic conditions. In the wing design optimization,

\* Graduate Student, Institute of Fluid Science

† Visiting Scientist, Institute of Fluid Science

‡ Associate Professor, Institute of Fluid Science, Associate Fellow AIAA

planform shapes, camber, thickness distributions and twist distributions were parameterized by 72 design variables. The resulting Pareto solutions were analyzed and compared with NAL's design.

Based on the wing design system mentioned above, an aerodynamic optimization system for SST wing-body configuration is developed in this research. To satisfy severe tradeoff between high aerodynamic performance and low sonic boom, the present objectives are to reduce  $C_D$  at a fixed  $C_L$  as well as to satisfy the equivalent area distribution for low sonic boom proposed by Darden.<sup>13</sup> Wing shape and fuselage configuration are defined in total of 131 design variables and are optimized at the same time. The wing definition is almost same as the previous wing optimization. 55 design variables are used to define nonsymmetric fuselage configuration. Four design variables represent the wing lofting. The multiblock grid approach is employed for aerodynamic evaluation. The junction line between wing and fuselage will be extracted to generate unstructured surface grid. Multiblock grids around SST wing-body configuration are then generated automatically based on the transfinite interpolation (TFI) method.<sup>14</sup> Multiblock Euler calculation is used to evaluate aerodynamic performance.<sup>15</sup> Master-slave type parallelization was performed to reduce the large computational time of each CFD evaluation in the optimization process.

## 2. Evolutionary Optimization

EAs, in particular GAs, are based on the theory of evolution, where a biological population evolves over generations to adapt to an environment by selection, crossover and mutation. In design optimization problems, fitness, individual and genes correspond to an objective function, design candidate and design variables, respectively. Figure 1 shows the common flowchart of GAs.

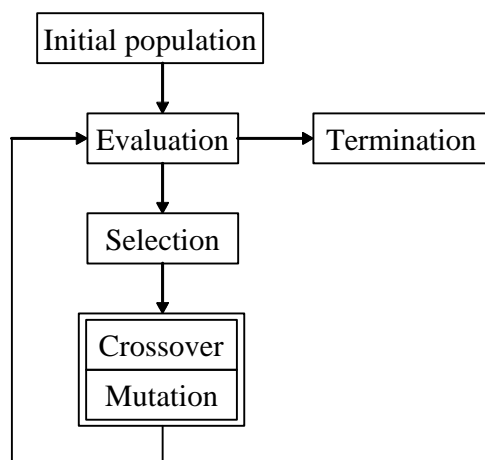


Fig. 1 Flowchart of GAs

## 2.1 Multiobjective GAs (MOGAs)

GAs search from multiple points in the design space simultaneously and stochastically, instead of moving from a single point deterministically like gradient-based methods. This feature prevents design candidates from settling in local optimum. Moreover, GAs do not require computing gradients of the objective function. These characteristics lead to following three advantages of GAs: 1, GAs have capability of finding global optimal solutions. 2, GAs can be processed in parallel. 3, High fidelity CFD codes can easily be adapted to GAs without any modification.

GAs have been extended to solve MO problems successfully.<sup>16,17</sup> GAs use a population to seek optimal solutions in parallel. This feature can be extended to seek Pareto solutions in parallel without specifying weights between the objective functions. The resultant Pareto solutions represent global tradeoffs. Therefore, MOGAs are quite unique and attractive methods to solve MO problems.

## 2.2 Real-Coded MOGAs

Traditionally, GAs use binary representation of design variables. For real function optimizations like the present aerodynamic optimization, however, it is more straightforward to use real numbers. Thus, the floating-point representation is used here.

Initial population is generated randomly. To prevent the large waste time of Euler computation, all individuals are generated so as to satisfy the constraints. If a candidate does not satisfy the constraints with 1% tolerance, a new candidate is generated again until it satisfies the constraints.

Selection is based on Fonseca's Pareto ranking method and fitness sharing.<sup>16</sup> Each individual is assigned to its rank according to the number of individuals that dominate it. A standard fitness sharing function is used to maintain the diversity of the population. To find the Pareto solutions more effectively, the so-called best- $N$  selection<sup>18</sup> is also coupled with. Finally, population of parents can be selected by Stochastic Universal Sampling (SUS) method based on fitness value calculated above.

Blended crossover (BLX- $\alpha$ )<sup>17</sup> described below is adopted. This operator generates children on a segment defined by two parents and a user specified parameter  $\alpha$ .

$$\begin{aligned}
 \text{Child1} &= \gamma \cdot \text{Parent1} + (1-\gamma) \cdot \text{Parent2} \\
 \text{Child2} &= (1-\gamma) \cdot \text{Parent1} + \gamma \cdot \text{Parent2} \\
 \gamma &= (1 + 2\alpha) \cdot \text{ran1} - \alpha
 \end{aligned} \tag{1}$$

where Child1,2 and Parent1,2 denote encoded design variables of the children (members of the new population) and parents (a mated pair of the old generation), respectively. Uniform random number  $\text{ran1}$  is defined in  $[0,1]$ . To prevent constraint violation, parameter  $\alpha$  is set to 0.0 during the present optimization. Polynomial mutation<sup>17</sup> is adopted as

mutation method. The disturbance is added to a new design variable at a mutation rate of 10%. If the mutation occurs, new design variable  $x_i'$  are obtained as

$$x_i' = x_i + (x_{UB,i} - x_{LB,i}) \cdot \delta_i \quad (2)$$

where  $x_i$  is original design variable,  $x_{UB,i}$ ,  $x_{LB,i}$  are upper and lower boundaries of the design variable, respectively. Parameter  $\delta_i$  is calculated based on the polynomial probability distribution.

$$\delta_i = \begin{cases} (2 \cdot \text{ran2})^{1/(\eta+1)} - 1 & (\text{ran2} < 0.5) \\ 1 - [2 \cdot (1 - \text{ran2})]^{1/(\eta+1)} & (\text{ran2} \geq 0.5) \end{cases} \quad (3)$$

where  $\text{ran2}$  is a uniform random number in  $[0,1]$ . A value of  $\eta$  decides a perturbation size of mutation and is set to 5.0. If a new candidate does not satisfy the constraints with the tolerance of 1%, it is generated again to prevent the waste time of evaluation.

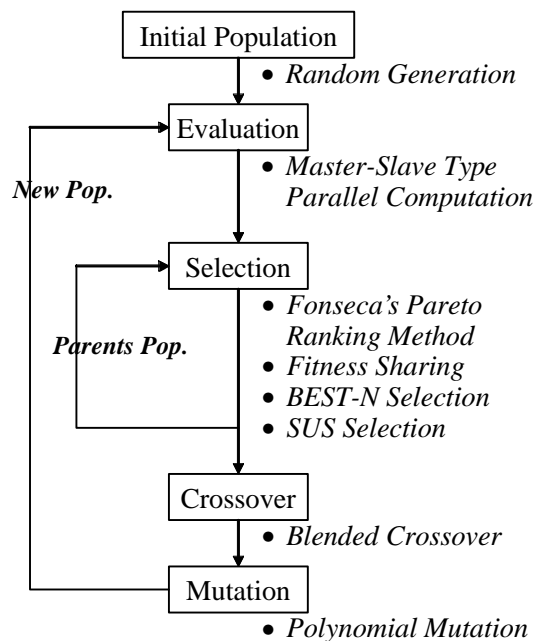


Fig. 2 Flowchart of present real-coded MOGAs

### 2.3 Master-Slave Type Parallelization

In general, MOGA with aerodynamic evaluation requires large computational time. Taking advantage of the characteristics of EAs for the reduction of computational time, the master-slave approach was taken for parallel processing of MOGAs on SGI ORIGIN2000 at the Institute of Fluid Science, Tohoku University. The master PE manages MOGA, while the slave PE's compute the multiblock Euler code for each individual. The population size was set to 64 so that the process was parallelized with 32-64 PE's depending on the availability. It should be noted that the parallelization was almost 100% because of the Euler computations dominated the CPU time.

## 3. Design Optimization System

### 3.1 NAL Design Contest

The present optimization is based on NAL's assignment. Design objective is to improve L/D at Mach number of 2.0 with a fixed  $C_L$  of 0.1. An optional objective is to reduce the sonic boom at Mach number of 1.6 with a fixed  $C_L$  of 0.125. Design specification of the present SST wing-body configuration is described in Table 1. The constraints are given based on the conceptual design for SST.

Table 1 Target SST wing-body specification

DESIGN OBJECTIVE:
<i>Reduction of drag (M2.0)</i>
DESIGN SPECIFICATION:
<i>Body length <math>\approx 300</math> ft</i>
<i>Body volume <math>\geq 30,000</math> ft<sup>3</sup></i>
<i>Minimum diameter <math>\geq 11.8</math> ft (<math>0.23 \leq x/L \leq 0.70</math>)</i>
<i>Wing area <math>\geq 9,000</math> ft<sup>2</sup></i>
<i>Wing volume <math>\geq 16,800</math> ft<sup>3</sup></i>
<i>Maximize t/c (extended root) <math>\geq 4\%</math></i>
<i>(other section) <math>\geq 3\%</math></i>
<i>Taper ratio <math>\approx 0.10</math></i>
<i>T.E. sweep angle (outboard) <math>\leq 30.0^\circ</math></i>
<i>Average structural sweep angle <math>\leq 48.0^\circ</math></i>
OPTION:
<i>Low boom configuration (M1.6)</i>

### 3.2 Problem Definition

In this study, SST wing-body configurations are designed to improve the aerodynamic performance and to lower the sonic boom strength. Therefore, design objectives are to reduce  $C_D$  at Mach number 2.0 at a fixed  $C_L$  ( $=0.10$ ) and to match Darden's equivalent area distribution that can achieve low sonic boom. To evaluate aerodynamic performances, aerodynamic evaluation has to be automatically performed for a given SST wing-body configuration. Therefore, a multiblock Euler solver is used in the present optimization, and figure 3 shows the flowchart of automated CFD evaluation from the given design variables. Geometries are at first determined based on the parameters and structured grids are then constructed around those configurations. Finally, Euler calculations are done for obtaining aerodynamic performances. Figure 4 shows the 30 multiblock grids around SST wing-body configuration. For the evaluation of sonic boom strength, an equivalent area distribution is adopted. The equivalent area distribution ( $Ae(t)$ ) can be calculated by the summation of equivalent cross sectional distribution ( $A(t)$ ) and lift distribution ( $B(t)$ ) as shown in Fig. 5. Figure 5 also shows Darden's equivalent area distribution for 300 ft fuselage SST at Mach number 1.6 at  $C_L = 0.125$ .

Constraints are also used in the optimization. As body length and wing area is fixed to 300 ft and 9,000 ft<sup>2</sup>, respectively, body volume, minimum diameter of body and wing volume must be greater than the values in Table 1. The other constraints are implemented as design variables.

Finally, the present SST wing-body design problem has two objective functions of minimization, three constraints and 131 design variables, and is optimized by real-coded MOGAs.

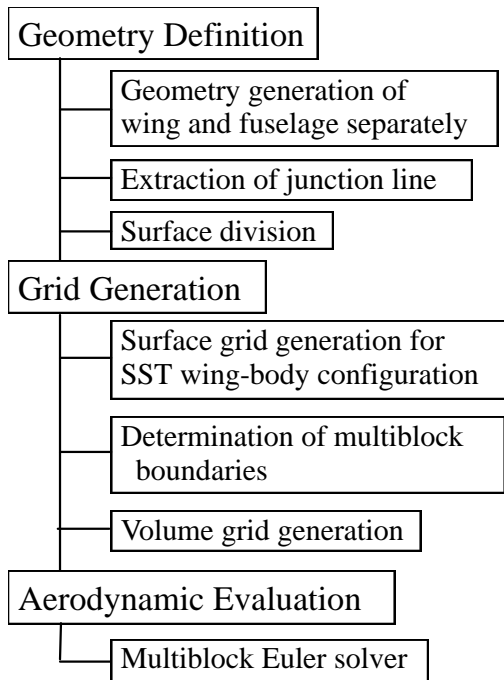


Fig. 4 Flowchart of automated CFD evaluation

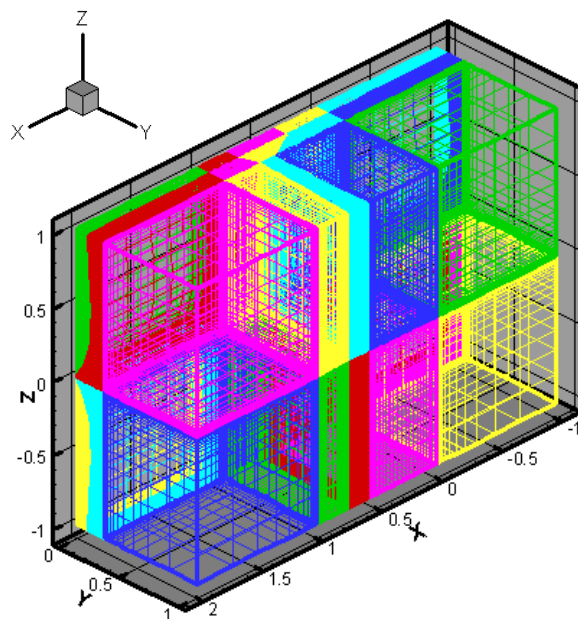


Fig. 5 30 multiblocks around SST wing-body configuration

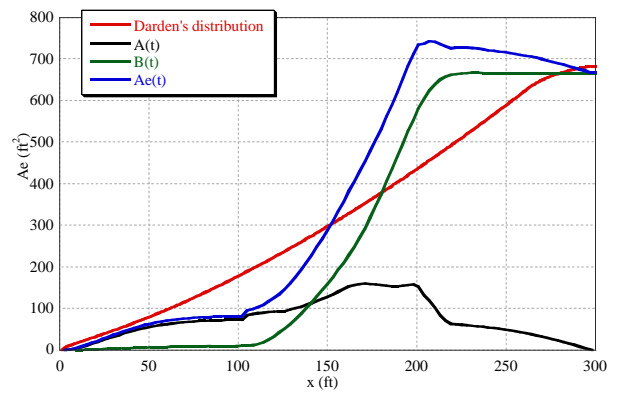


Fig. 6 Equivalent area distribution of Darden's and designed geometry

### 3.3 Geometry Definition

Design variables, which determine the shape of wing-body configurations here, are composed of three groups: wing shape, fuselage configuration and wing lofting. Design variables for the wing shape is categorized to planform, warp shape and thickness distribution. The warp shape is composed of camber and twist distributions. Figure 7 shows the definition of the planform shape based on 6 design variables: inboard and outboard spanwise lengths, chordwise lengths at kink and tip, inboard average structural sweepback angle and outboard trailing-edge sweepback angle. Bézier surfaces and B-Spline are used to represent camber, twist and thickness distributions.<sup>10</sup> Fuselage configuration is defined by a Bézier surface with 37 polygons to represent complex non-axisymmetric configuration. Five design sections in the  $x$ -direction are used, where seven polygons are defined at each section as shown in Fig. 8. 37 polygons correspond to 55 design variables after imposing geometric constraints to the fuselage. Four design variables are used for the wing lofting that indicates how to combine wing and fuselage. Design variables are incidence, location of extended wing root and dihedral as shown in Fig. 9. The total number of design variables is 131.

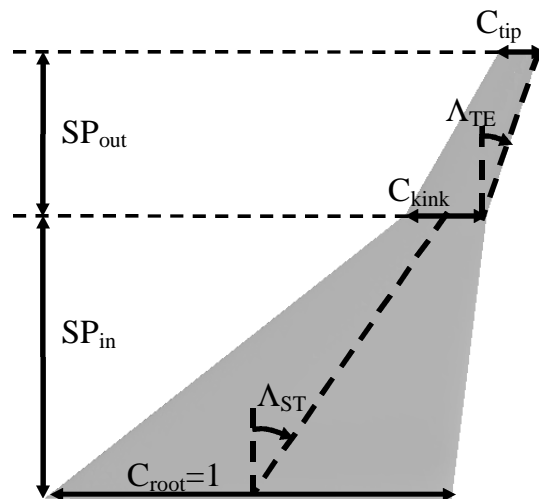
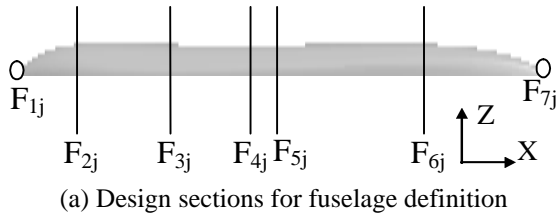
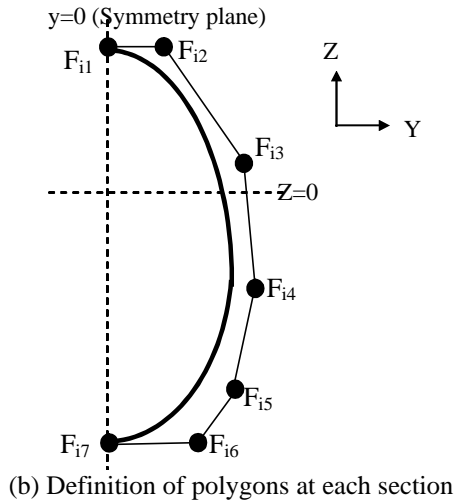


Fig. 7 Planform shape definition



(a) Design sections for fuselage definition



(b) Definition of polygons at each section

Fig. 8 Fuselage definition

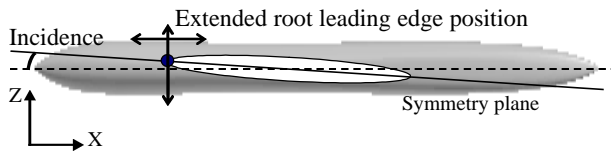
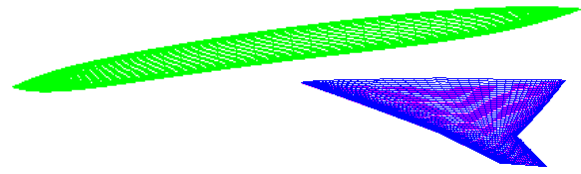


Fig. 9 Wing lofting definition

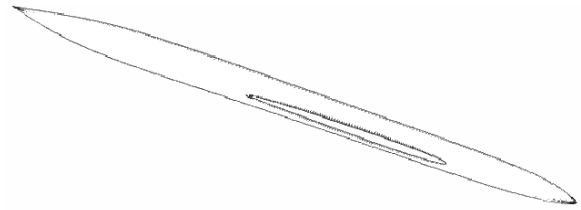
### 3.4 Grid Generation

To generate a surface grid, a junction line between wing and fuselage has to be extracted efficiently. For this purpose, structured grids for wing and fuselage are separately generated at first (Fig. 10 (a)). The grid lines on fuselage surface that intersect the wing surface are then searched efficiently by Lawson's search,<sup>19</sup> resulting the junction line (Fig. 10 (b)). According to the junction line, eight surface patches on the wing-body configuration are determined for the generation of multiblock grids (Fig. 10 (c)).

From the surface patches determined above, block boundaries are easily defined for the volume grid generation. Figure 10 (d) shows the generated surface grid on wing and fuselage, respectively. Finally, volume grid can be generated by TFI method. Figure 5 shows the resulting 30 block grids around the SST wing-body configuration. Figure 12 shows sample wing-body configurations and the corresponding surface grids.



(a) Surface grid for wing and fuselage



(b) Junction line between wing and fuselage



(c) Division of wing-body configuration



(d) Re-generated surface grid for wing and fuselage

Fig. 10 Generation of surface grid on SST wing-body configuration

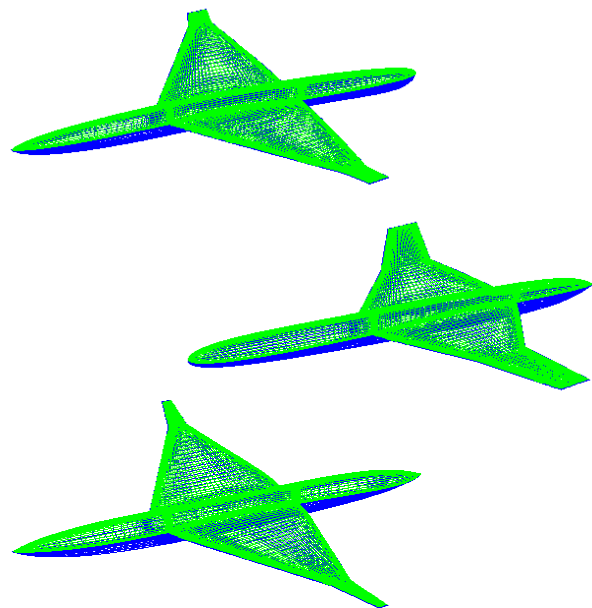


Fig. 11 Sample wing-body configurations with surface grids

### 3.5 Aerodynamic Evaluation

For the present aerodynamic evaluation, multiblock Euler calculation<sup>15</sup> is performed. This Euler solver employs total-variation-diminishing type upwind differencing and the lower-upper factored symmetric Gauss-Seidel (LU-SGS) scheme<sup>20</sup>. To maintain lift coefficients constant, the angle of attack is predicted by using  $C_{L\alpha}$  obtained from the finite difference. Thus, three Euler computations are performed per evaluation. It requires nearly six hours for one evaluation using a single PE of ORIGN2000.

## 4. Optimization Results

### 4.1 CASE I Design Results

The present optimization was performed for 20 generations and the resulting non-dominated solutions were considered as Pareto solutions. In Fig. 10, non-dominated solutions in the initial, 10th, and 20th populations are shown. In the figure, the vertical axis is the difference of equivalent area distribution from Darden's distribution. If the difference is small, then it indicates a theoretically low boom design. The Pareto front obtained from the 20th population represents the tradeoff between drag and boom. Several wing-body configurations of the Pareto solutions are also presented in the figure. In case of the initial designs, comparatively various kinds of wing-body configuration were generated. On the other hand, the final Pareto solutions have similar wing planforms.

Extreme Pareto solutions are chosen for comparison: the lowest drag (LD-I) and the lowest boom (LB-I). Table 2 shows their aerodynamic performances and design features. In addition, their planforms and the side views of their fuselages are shown in Fig. 13. Their planform shapes appear similar because the constraint on the wing volume is very severe and thus the planform is not allowed to change drastically. On the contrary, fuselage shapes are found to have a variety. As shown in Fig. 13, LB-I has similar distribution to Darden's especially in the fore body by getting thicker. In contrast, LD-I's distribution is totally different from Darden's and the fuselage shape appears thinner.

Although LD-I has the highest L/D, its value does not appear excellent. To improve L/D more, fuselage configurations must be more slender than those of the present solutions. This indicates that MOGAs have to search solutions near the geometric constraints on the fuselage. However, the present MOGAs did not focus in such a region, and the solutions tend to have a thick fuselage.

Table 2 Aerodynamic performances and design specifications of selected Pareto solutions (Case I)

	LD-I	LB-I	Constraints
L/D	11.1	8.1	
Difference of $Ae(t)$	6569	3428	
Body volume (ft <sup>3</sup> )	43798	62085	30000
Min. diameter (ft)	11.97	15.74	11.8
Wing volume (ft <sup>3</sup> )	18397	17441	16800

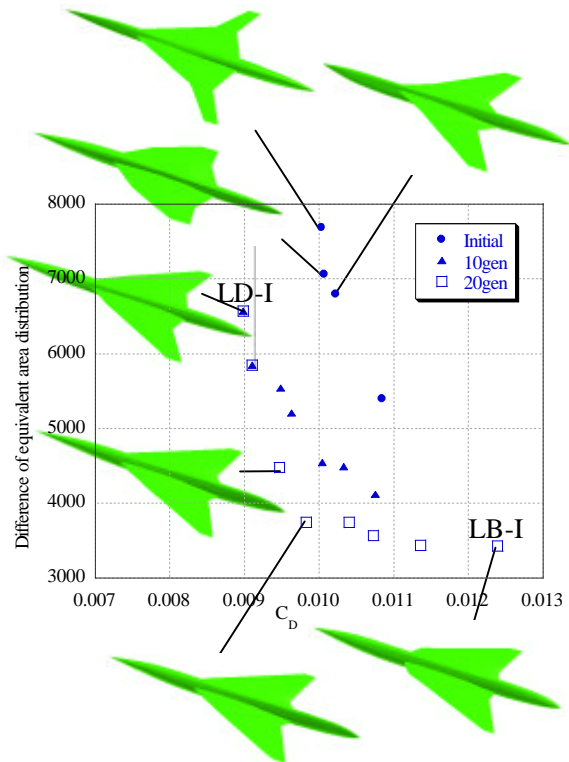
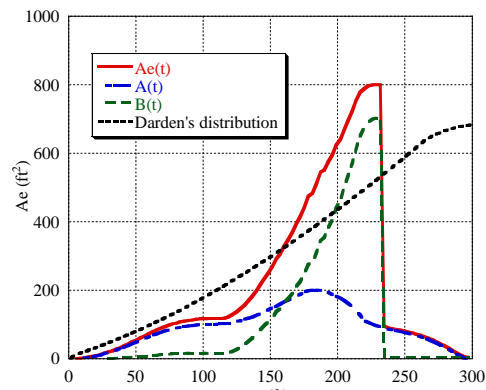
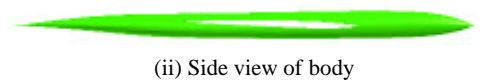
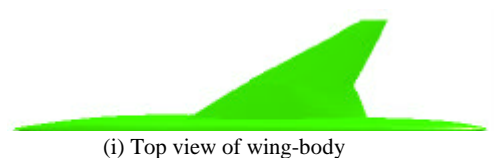


Fig. 12 Non-dominated solutions of initial, 10th and 20th generation with some wing-body configurations



(a) LD-I

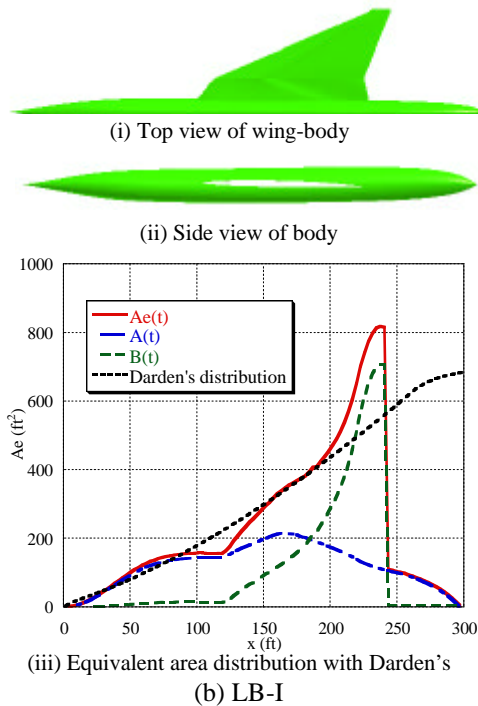


Fig. 13 Wing-body shapes and equivalent area distributions of selected Pareto solutions

#### 4.2 CASE II Design Results

From a result of the optimization in Sec.4.1, fuselage configuration has to be thin to obtain high aerodynamic performance. Therefore, the upper bound is imposed onto the fuselage volume as described in Table 3.

Similar aerodynamic optimization with a new constraint was performed for 20 generations. In Fig. 14, non-dominated solutions in the initial, 10th, and 20th populations are shown. Several wing-body configurations of the Pareto solutions are also presented in the figure. In this optimization, from the beginning, those designs have better aerodynamic performances than Case I optimization. All the wing shapes of non-dominated initial designs are similar. For the final Pareto solutions, planform shapes are also quite similar. The drag coefficients are improved over 10 counts compared with those of CASE I.

Extreme Pareto solutions are chosen for comparison: the lowest drag (LD-II) and the lowest boom (LB-II). Table 4 shows their aerodynamic performances and design features. In addition, their planforms and the side views of their fuselages are shown in Fig. 15. Their planform and fuselage configurations appear similar. Only the difference is the thickness distribution near the nose of fuselage. It results in a difference of low drag or low boom.

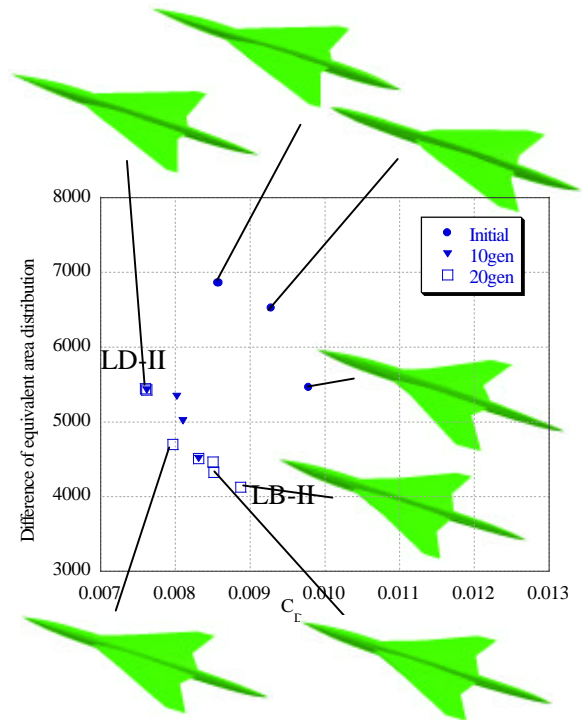
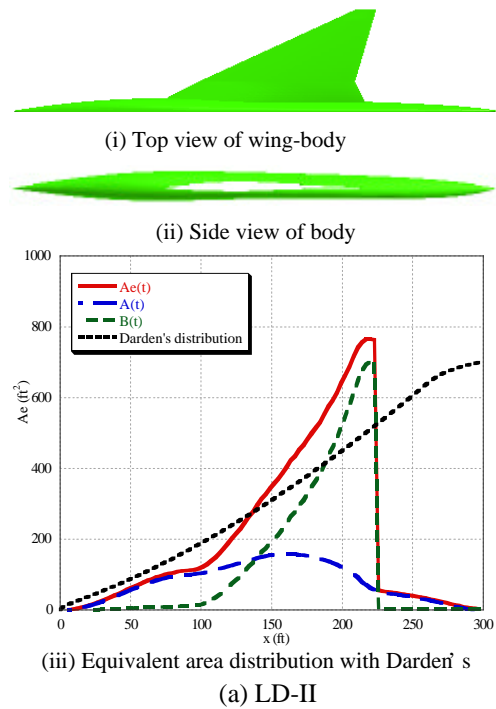


Fig. 14 Non-dominated solutions of initial, 10th and 20th generation with some wing-body configurations (Case II)



(iii) Equivalent area distribution with Darden's (a) LD-II

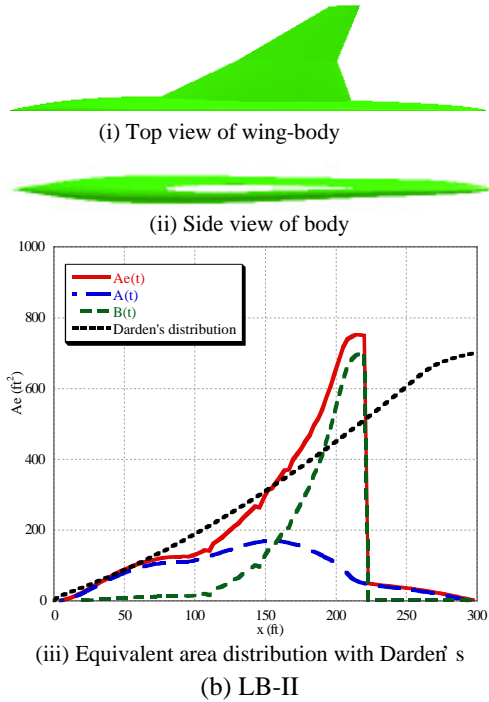


Fig.15 Wing-body shapes and equivalent area distributions of selected Pareto solutions

Table 3 Constraints for Case II

DESIGN CONSTRAINTS:

$$40,000\text{ft}^3 \geq \text{Body volume} \geq 30,000\text{ft}^3$$

$$\text{Minimum diameter} \geq 11.8\text{ ft } (0.23 \leq x/L \leq 0.70)$$

$$\text{Wing volume} \geq 16,800\text{ft}^3$$

Table 4 Aerodynamic performances and design specifications of selected Pareto solutions (Case II)

	LD-II	LB-II	Constraints
L/D	13.10	11.24	
Difference of $Ae(t)$	5427	4124	
Body volume ( $\text{ft}^3$ )	34379	37688	30000
Min. diameter (ft)	11.75	12.29	11.8
Wing volume ( $\text{ft}^3$ )	19337	20889	16800

### 4.3 Comparison of Pareto Solutions

Both Pareto solutions (Case I and II) are discussed in this section. Pareto solutions (Case I and II) are shown in Fig. 16. It is easily found that LD-I and LB-II have similar drag coefficients but a large difference in the equivalent area distribution. The shape difference is only the distributions of fuselage thickness. From the nose of the fuselage to the trailing edge of the wing is considered for the equivalent area distribution in the present optimization. Therefore, a more detailed analysis may be required to obtain accurate sonic boom in future.

Solution LB-I has the increased fuselage volume for the low boom at the cost of the increased drag. It

indicates that, if the fuselage volume is constrained to the original size to maintain its aerodynamic efficiency, there is no way to match Darden's distribution under the present constraints on the wing. The present result therefore suggests that the lifting surface should be distributed along the fuselage for low boom and low drag. The low boom supersonic aircraft should have an innovative planform shape.

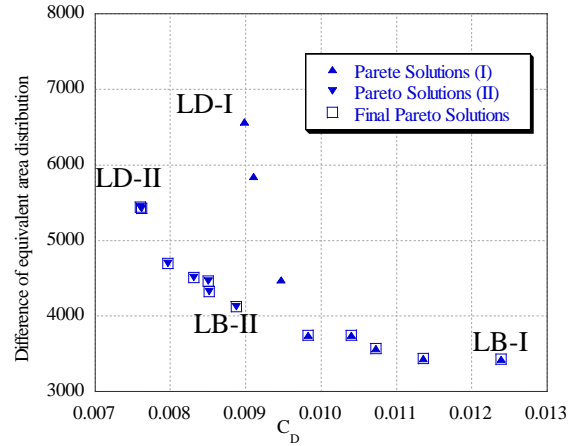


Fig.16 Comparison of Pareto solutions between Case I and II.

## 5. Conclusion

Design optimization for SST wing-body configurations was performed based on NAL design competition. Design objectives were to improve aerodynamic performance at Mach number 2.0 and to reduce sonic boom at Mach number 1.6. These two objectives were optimized by using MOGAs. To evaluate aerodynamic performance, an Euler calculation was used. The sonic boom was evaluated according to Darden's distribution. Each evaluation was parallelized on SGI ORIGIN2000 at the Institute of Fluid Science, Tohoku University.

Multiblock grid was used to treat a complex geometry of SST wing-body configuration. Geometry is defined by in total of 131 design variables. Based on these design variables, multiblock grids were automatically generated around SST wing-body configuration by Lawson's search and TFI method.

As a result of Case I, 8 Pareto solutions were obtained. Extreme Pareto solutions were chosen for comparison. The design of lowest boom has a thick fuselage to match Darden's distribution. On the other hand, excellent improvement in L/D was not obtained for lowest drag design because MOGAs were not able to search near the constraint boundary and all designs have thick fuselage.

To improve L/D, the upper bound for fuselage volume was introduced in Case II. Aerodynamic performances were improved successfully; however, a drastic improvement in L/D was not obtained due

to the severe constraints.

Although the resulting Pareto solutions in both cases have a variety of fuselage configurations, they have a similar planform for wing shapes. Because a similar wing planform leads to a similar lift distribution, the fore body has to become thick to match Darden's distribution for low boom. Thus, the low boom optimization simply resulted in a thick fuselage with poor aerodynamic performance. The present result suggests that a lifting surface should be distributed innovatively to reduce both boom and drag, which will result in unconventional wing-fuselage configurations. In addition, to improve the aerodynamic performance further, MOGAs have to focus at the boundary of geometric constraints better. The constraint handling in MOGA remains for future research.

### Acknowledgements

The present computation was carried out in parallel using ORIGIN2000 in the Institute of Fluid Science, Tohoku University. The authors would like to thank Dr. Yoshida and NAL's SST Design Team for providing many useful data.

### References

- [1] Alonso, J. J., Kroo, I. M. and Jameson, A., "Advanced Algorithms for Design and Optimization of Quiet Supersonic Platforms," AIAA Paper 2002-0144, January 2002.
- [2] Cliff, S. E., Reuter, J. J., Saunders, D. A. and Hicks, R. M., "Single-Point and Multipoint Aerodynamic Shape Optimization of High-Speed Civil Transport," *Journal of Aircraft*, Vol.38, No.6, pp.997-1005, 2001.
- [3] Sakata, K., "Supersonic Experimental Airplane (NEXST) for Next Generation SST Technology," AIAA Paper 2002-0527, January 2002.
- [4] Shimbo, Y., Yoshida, K., Iwamiya, T., Takaki, R. and Matsushima, K., "Aerodynamic Design of Scaled Supersonic Experimental Airplane," *Proc. of 1st SST-CFD Workshop*, pp.62-67, 1998.
- [5] Iwamiya, T., Yoshida, K., Shimbo, Y., Makino, Y. and Matsuhima, K., "Aerodynamic Design of Supersonic Experimental Airplane," *Proc. of 2nd SST-CFD Workshop*, pp.79-84, 2000.
- [6] Makino, Y. and Iwamiya, T., "Aerodynamic Nacelle Shape Optimization for NAL's Experimental Airplane," *Proc. of 2nd SST-CFD Workshop*, pp.115-120, 2000.
- [7] Grenon, R., "Numerical Optimization in Aerodynamic Design with Application to a Supersonic Transport Aircraft," *Proc. of 1st SST-CFD Workshop*, pp.83-104, 1998.
- [8] Kim, H.-J., Sasaki, D., Obayashi, S. and Nakahashi, K., "Aerodynamic Optimization of Supersonic Transport Wing Using Unstructured Adjoint Method," *AIAA Journal*, Vol.39, No.6, pp.1011-1020, June 2001.
- [9] Obayashi, S., Sasaki, D., Takeguchi, Y. and Hirose, N., "Multiobjective Evolutionary Computation for Supersonic Wing-Shape Optimization," *IEEE Transactions on Evolutionary Computation*, Vol.4, No.2, pp.182-187, 2000.
- [10] Sasaki, D., Obayashi, S. and Nakahashi, K., "Navier-Stokes Optimization of Supersonic Wings with Four Objectives Using Evolutionary Algorithm," *Journal of Aircraft*, vol.39, No.4, pp.621-629.
- [11] Vicini, A. and Quagliarella, D., "Multipoint Transonic Airfoil Design by Means of a Multiobjective Genetic Algorithm," AIAA 97-0082, 1997.
- [12] Oyama, A., Obayashi, S. and Nakamura, T., "Real-Coded Adaptive Range Genetic Algorithm Applied to Transonic Wing Optimization," *Applied Soft Computing*, Vol.1, No.3, pp.179-187, 2001.
- [13] Darden, C. M., "Sonic Boom Theory: Its Status in Prediction and Minimization," *Journal of Aircraft*, Vol.14, No.6, pp.569-576, 1977.
- [14] Jones, W. T., "A grid Generation System for Multi-Disciplinary Design Optimization," AIAA Paper 97-2039, 1997.
- [15] Yang, G., Kondo, M. and Obayashi, S., "Multiblock Navier-Stokes Solver for Wing/Fuselage Transport Aircraft," *JSME International Journal*, Series B, Vol.45, No.1, pp.85-90, 2002.
- [16] Fonseca, C. M. and Fleming, P. J., "Genetic Algorithms for Multiobjective Optimization: Formulation, Discussion and Generalization," *Proc. of 5<sup>th</sup> ICGA*, pp.416-423, 1993.
- [17] Deb, K., *Multi-Objective Optimization using Evolutionary Algorithms*, John Wiley & Sons, Ltd., Chichester, 2001.
- [18] Obayashi, S., Takahashi, S. and Takeguchi, Y., "Niching and Elitist Models for MOGAs," Parallel Problem Solving from Nature – PPSN V, *Lecture Notes in Computer Science*, Springer, Berlin Heidelberg New York, pp.260-269, 1998.
- [19] Taniguchi, T., *Automatic Element Division for FEM*, Morikita publishing house, Tokyo, 1992 (in Japanese).
- [20] Yoon, S. and Jameson, A., "Lower-Upper Symmetric-Gauss-Seidel Method for the Euler and Navier-Stokes Equations," *AIAA Journal*, Vol.26, pp.1025-1026, 1988.